Advances in Science and Technology Research Journal

Advances in Science and Technology Research Journal, 2025, 19(11), 275–291
https://doi.org/10.12913/22998624/209577
ISSN 2299-8624, License CC-BY 4.0

Received: 2025.06.30
Accepted: 2025.09.15
Published: 2025.10.01

Comparison of cavitation erosion and sliding wear resistance of welded CoCrWC and NiCrBSi hardfacings, AISI 316L stainless steel, and S235JR mild steel

Mirosław Szala[1*], Mariusz Walczak[1], Tomasz Pałka[1], Maciej Kowal[2], Wojciech J. Nowak[3]

[1] Faculty of Mechanical Engineering, Lublin University of Technology, Nadbystrzycka 36D, Lublin 20-618, Poland
[2] Faculty of Civil Engineering and Architecture, Lublin University of Technology, Nadbystrzycka 40, 20-618 Lublin, Poland
[3] Faculty of Mechanical Engineering and Aeronautics, Rzeszow University of Technology, Powstanców Warszawy 12, Rzeszów, Poland
* Corresponding author's e-mail: m.szala@pollub.pl

ABSTRACT

The main objective of the study was to comparatively analyse the cavitation erosion resistance and dry sliding wear resistance of two hardfacing alloys: NiCrBSi (a self-fluxing alloy) and CoCrWC (Stellite 6), as well as two popular steels – S235JR mild steel (approx. 0.17% C) and stainless steel (AISI 316L). CoCrWC was hardfaced using the TIG (tungsten inert gas) welding method and NiCrBSi using the oxy-flame powder welding method on a mild steel substrate. Cavitation studies were carried out according to ASTM G32 standard with a standoff of 0.5 mm. Sliding wear resistance tests were carried out using the ball-on-disc method (100Cr6 steel counterball). CoCrWC hardfacing shows the highest cavitation erosion and sliding wear resistance. Therefore, the maximum depth of erosion rate was the lowest for CoCrWC < NiCrBSi < AISI 316L < S235JR. Sliding wear resistance is shown in the following order, starting with the minimal material loss: CoCrWC > NiCrBSi > S235JR > AISI 316L. The lowest coefficient of friction (COF) was observed for S235JR (COF=0.467), while the other samples exhibited comparable COF values in the range 0.605–0.698. Microstructure and hardness ratio critically affect wear; accordingly, soft single-phase materials suffer high losses in sliding wear and cavitation erosion tests. Wear mechanisms were studied using SEM. Cavitation erosion resistance relies on the metallic matrix's capacity to absorb loads and resist fatigue. Erosion begins with deformation of the metallic phase at phase interfaces, leading to detachment of the weakened material. In hardfacings, carbides and borides are dislodged once they lose support, ultimately forming pits, craters, and cracks through fatigue-induced detachment. Sliding wear behaviour is dictated by microstructure. Hard particles embedded in a matrix minimise abrasive wear and reduce material loss. In contrast, soft, single-phase steels undergo abrasive wear debris accumulation, leading to adhesive wear, raising wear rates. AISI 316L suffers the highest wear – its oxidised debris spalls off – whereas S235JR benefits from a well-adhering tribofilm and lower material loss. CoCrWC and NiCrBSi coatings showed higher cavitation and sliding wear resistance than reference steels.

Keywords: cavitation erosion, cavitation corrosion, tribology, Stellite 6, ball-on-disc, stainless steel, steel, failure analysis.

INTRODUCTION

The components that operate in cavitation erosion or sliding wear environments are produced by machining, casting, and metal forming from various metal alloys. In specific applications, such as centrifugal pumps, water turbines or pipeline valves, the material should withstand both sliding wear and cavitation erosion loads [1,2]. Thus, the candidates for these materials are cobalt- and nickel-based alloys, which successfully compete with stainless steel.

Their high strength, hardness and wear resistance, impact strength, resistance to corrosion, and elevated temperature make them widely used in the production and regeneration of machine parts [3,4]. On the other hand, nickel and cobalt-rich materials are relatively expensive, and cost-effective solutions are the use of mild or stainless steels. The appropriate design and cost-effective selection of materials are crucial for prolonging the operation time of engineering systems. Thus, a comparative analysis of the wear performance of nickel and cobalt-based hardfacings with steels is required.

S235JR steel is widely used in mild steel applications due to its favourable mechanical properties, machinability and cost-effectiveness. Stainless steel grades 304 or 316 are well formable and widely used where corrosion resistance is needed [3,5]. Alloys with a matrix of iron, cobalt and nickel are generally used to produce wear-resistant layers using welding technologies. Still, the hardfacing of ferrous overlays is the dominant method for prolonging the operation performance of different machines [6,7], and various methods of hardfacing are employed [8–10]. Tribological behaviour of steels is well presented in the literature [11–13]. Low-carbon steel, such as S235JR steel, has poor anti-wear performance [11]. Sometimes it is recommended to be replaced by stainless steel AISI 304, but exemplary in abrasive wear conditions, depending on the used abrasive, it can give a very poor performance [14]. Systematically, the other metallic materials or coatings are tested in a wet [15–17] and dry sliding wear [18,19] environment. Especially surface modification, likewise, laser cladding [20] or ion-implantation [21,22] or cermets coatings deposition [23], among others, are studied. Even though the development of additive manufactured components for anti-wear applications has been ongoing, welding methods remain indispensable in certain applications. The stainless steel [24–26] or low-carbon structural steel [27, 28] components are well fabricable by additive manufacturing, but the materials such as cobalt-based alloys or nickel are not typically manufactured by additive manufacturing. The plastic forming and CNC machining of steel are well operated, but metallic components and coatings made of Stellite 6 or NiCrBSi are considered challenging to shape in conventional industrial conditions [29–31]. The directed energy deposition (DED) methods [32,33] are investigated to build up the Stellite 6 components. Although still, the main deposition methods of Stellite 6 and NiCrBSi coatings for wear-preventing applications are still welding [18,34,35] or thermal spraying methods [30,36]. However, comparative data on the wear behavior of nickel- and cobalt-based hardfacings remain scarce, especially when tested in reference to mild steel and stainless steels, which is fulfilled by the results presented in this research.

The materials used in anti-cavitation erosion applications are mostly austenitic [37] or martensitic [38] stainless steels [39], bronzes [40] and cermet [41], polymer [42] or shape memory alloy coatings [43]. Systematic investigations relating to the erosion resistance of other new materials are published in the literature. Literature data and own research show the possibility of increasing the durability of elements many times by using wear-resistant coatings [5] or modifying the surface layer to produce, using various techniques to prevent erosion or sliding of the in-situ TiC hardfacings [44] or TiC layers [45] that are deposited. Likewise, the cavitation erosion resistance of sintered stainless steel 316L was compared with the shape memory alloy Cu-12.8Al-4.1Ni [46], which shows far more resistance to cavitation erosion.

An increasing number of studies compare the cavitation erosion resistance of different engineering materials, but few present comprehensive data on both sliding wear resistance and cavitation erosion resistance. For example, in the work [47] the tribological and cavitation erosion behaviours of nickel-based and iron-based coatings deposited on AISI 304 stainless steel by cold metal transfer are examined. GTAW hardfacing for the nuclear power industry, Co-base Stellite 6 and new Fe-base alloys were comparatively investigated [48], resulting in the highest erosion resistance of ferrous hardfacing Fe-20Cr-1.6C-1Si noted after 150 hours of exposure to cavitation. However, until 100 hours of exposure, Stellite 6 coating notes lower mass loss than the ferrous one. In the work [49], the cavitation erosion and wear resistance of high-alloy WC coatings produced by electric arc spraying were revealed to be promising for reducing wear on mild steel substrates. Finally, in the works [50–52], the erosion resistance of different grades of stainless steels, Hatfield, martensitic, and mild steels, was examined.

Unfortunately, there is no comprehensive work combining data on the anti-wear performance of mild steel, stainless steel, cobalt, and nickel hardfacings, which have been tested under cavitation erosion and dry sliding wear conditions.

The aim of this work is to compare and evaluate the cavitation erosion and dry sliding wear resistance of two popular steels, namely S235JR mild steel (approximately 0.17% C) and stainless steel (AISI 316L), along with the weld hardfacings NiCrBSi (self-fluxing alloy) and CoCrWC (Stellite 6).

MATERIAL AND METHODS

Characteristics of investigated materials

The tests were carried out on samples made of S235JR mild steel, AISI 316L stainless steel and hardfacings NiCrBSi and CoCrWC. The chemical composition of the commercial feedstock materials used to prepare the hardfacings is shown in Table 1. The cobalt-based hardfacing (CoCrWC, Stellite 6) was applied in three layers on the S235JR steel substrate to minimise dilution. The tungsten inert gas (TIG) welding employing a non-consumable tungsten electrode in an inert gas shielded (argon) process no. 141, according to EN ISO 4063, was used. The filler material was a solid rod, Ø 3.2 mm. The nickel-based hardfacing (NiCrBSi, Deloro 60) was prepared onto the S235JR substrate using the oxy-acetylene powder hardfacing method, which itself guarantees minimal dilution. Then the surfaces of the coatings were machined and ground to obtain a flat surface. The samples for the cavitation erosion and dry sliding wear testing were machined to obtain dimensions of Ø30 × 7 mm. Then, it was polished to achieve the roughness of Sa < 0.06 µm and Sz < 0.72 µm. The microstructure was analysed using SEM method. The hardness of the samples and hardfacings was measured using the Vickers method at a load of 0.5 kg, i.e. HV0.5, with an indentation dwelling time of 10 seconds, following ISO 6507 standard procedure.

Cavitation erosion testing

The stationary specimen method was used to test cavitation erosion resistance, following the ASTM G32 standard. The scheme of the test stand is shown in Figure 1. A titanium sonotrode tip (Ø 15.9 mm) vibrating in distilled water generated a cavitation field, which affected the surface of the sample mounted in a fixed standoff from the vibrating horn. Detailed test conditions are reported in Table 2. The targeted total exposure time was 35 hours. Samples were weighed at specified time intervals, which served as the basis for estimating cavitation erosion curves, presenting the mean depth of erosion MDE (µm), Equation 1, and the mean depth of erosion rate, MDER (µm·h^{-1}) versus time of exposure to cavitation. Then, the maximum of the mean depth of erosion rate, $MDER_{max}$, was noted as the maximum instantaneous erosion rate in a test that exhibits such a maximum, followed by a decreasing erosion rate. The surfaces after erosion testing were examined using a Phenom ProX scanning electron microscope (SEM, Phenom-World, Waltham, MA, USA) using BSE and topographic modes.

$$Mean\ depth\ of\ erosion, MDE = \\ = \frac{Mass\ loss}{Material\ density \times erosion\ area}, (\mu m) \quad (1)$$

Tribological testing

Sliding wear tests were performed at room temperature using a ball-on-disc tribometer. A counterball made of hardened 100Cr6 bearing steel loads

Table 1. Nominal chemical composition of the hardfacings and commercial steels

Sample	Chemical element and content, wt.%												
	Fe	Ni	Co	Cr	W	Mo	C	B	Si	Mn	P	S	N
CoCrWC (Stellite 6)	2.5	-	Bal.	28	4.5	-	1.1	-	1.0	0.6	-	-	
NiCrBSi (Deloro 60)	3.5	Bal.	-	15	-	-	0.75	3.2	4.4	-	-	-	
S235JR (1.0037)	Bal.	-	-	-	-	-	0.17	-	<0.35	<1.40	<0.045	<0.045	<0.009
AISI 316L (1.4401)	Bal.	10.00–13.00	-	16.50–18.50	-	2.00–2.50	<0.03	-	<1.0	<2.00	<0.045	<0.015	<0.10

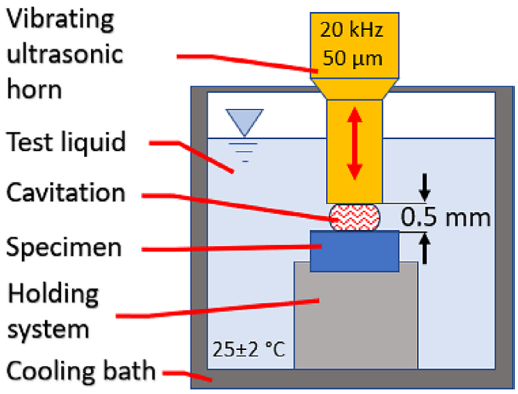

Figure 1. Idea of the cavitation erosion testing

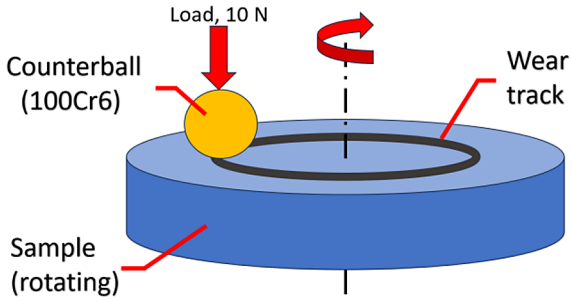

Figure 2. Idea of the sliding wear testing

Table 2. Cavitation erosion test conditions

Test parameter	Value
Horn vibration frequency	20 kHz
Horn vibration amplitude	50 µm
Sonotrode tip – sample standoff	0.5 ± 0.05 mm
Distilled water temperature	25 ± 2 °C

the surface of the rotating tested sample, Figure 2. The sample was rotated at a specific sliding velocity to obtain the sliding distance, as listed in Table 3. Moreover, the coefficient of friction (COF) was recorded during each test. The wear was determined based on the wear rate *K,* which was calculated using the Archard equation [53], Equation 2. After executing tribological testing, the wear track of the examined materials was evaluated using scanning electron microscopy (SEM).

$$Wear\ rate, K = \\ = \frac{Volume\ loss}{Applied\ load\ \times\ sliding\ distance}, \quad (2)$$

$$(mm^3 N^{-1} m^{-1})$$

RESULTS AND DISCUSSION

Characteristics of investigated materials

The microstructure and hardness of the investigated materials are compared in Figures 3 and 4, respectively. The microstructure of the hardfacings is significantly more complex than the phase composition of the investigated steels. CoCrWC (Stellite 6) hardfacing displays a dense structure with no pores or cracks. Its microstructure consists of a cobalt-based solid solution γ-(Co) dendrites, where, according to the literature [54,55], it is dominated by face-centred cubic (FCC) structure. At the first stage of solidification, the γ-(Co) phase is dendritically formed. Then, the interdendritic regions and eutectic carbides rich in Cr and C, such as $Cr_{23}C_6$, are formed, as well as the W-rich phases (white areas in Figure 3a). Therefore, the mean hardness of the coating was 531 HV 0.5, see Figure 4. The conducted microstructure and hardness analysis confirm that the TIG-deposited CoCrWC coating shows comparable results to those obtained with different deposition techniques [32,33,55,56] likewise reported hardness of 547 HV0.2 [32] and 522 ± 21 HV0.3 [33].

The phase composition of the NiCrBSi is much more complex than that of the other tested materials, see Figure 3b. It consists of a nickel-based solid solution γ-(Ni, Fe) along with various dispersed hard phases such as borides, carbides, boron carbides, silicides and different eutectics. Typical phases reported in the literature [57] include CrB, Cr_3C_2, M_7C_3 (M = Cr, Fe, and Ni), Ni_3B, and $Cr_{23}C_6$, Ni_3Si and $CrSi_2$, as well as Ni-Ni_3Si and Ni-Ni_3B eutectics [58]. The solid solution provides the base for the coating's mechanical properties, while the hard phases are present in the microstructure in a clustered form, which contributes to the highest hardness of 748 HV 0.5, see Figure 4. The measured hardness and results of microstructure analysis are comparable to those of other studies done for comparable NiCrBSi hardfacings, manufactured by laser cladding [59], plasma powder [60] or the oxy-acetylene powder deposition method [61].

Following the literature, the microstructure of mild steel S235JR is characterized as ferritic-pearlitic (Figure 3c), with ferrite being predominant and pearlite grains located along the boundaries of the ferrite grains. Ferrite is known to have lower

Table 3. Dry sliding wear testing conditions

Test parameter	Value
Applied load	10 N
Linear velocity	3.77 cm/s
Radius of the wear track	3 mm
Sliding distance	100 m
Counterball (steel 100Cr6, 64 HRC, approx. 800 HV)	Ø 6 mm

hardness than pearlite, and the overall hardness of steel has been reported as 135 HV0.5. The AISI 316L stainless steel microstructure is single-phase austenitic, consisting of annealing twins and alloying elements uniformly distributed throughout the austenite grains (Figure 3d). The hardness of stainless steel typically relates to its deformation ratio, and hardness measurements indicated a 282 HV 0.5. Investigated steel's microstructure and hardness align with values documented in previous studies relating to AISI 316 and AISI 304 [3,62,63] stainless steels. On the other hand, it should be noted that the hardness of AISI 316L steel depends on the surface layer preparation (grinding or polishing) [64], and the hardness is increased by using a coarser grinding medium [65].

Overall, the microstructure of metal alloys has a significant influence on their hardness (Figure 4). Therefore, the highest hardness was noted for NiCrBSi, CoCrWC, AISI 316L and S235JR, respectively. The thematic literature considers the microstructure and hardness as main factors influencing the cavitation erosion resistance and sliding wear behaviour of metallic structures [66,67].

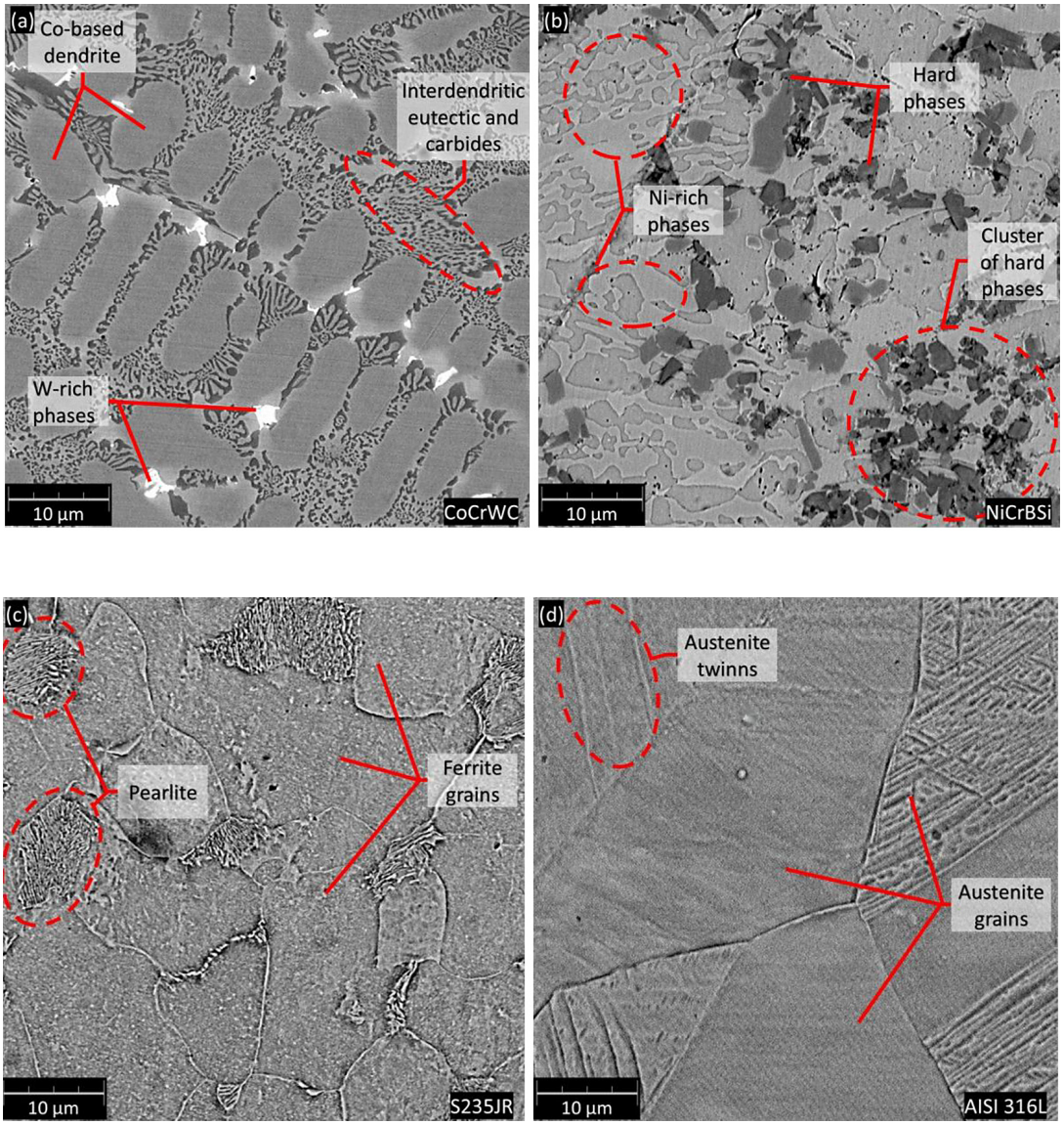

Figure 3. Microstructure of hardfacings (a, b) and reference steels (c, d), mag. x5000, SEM

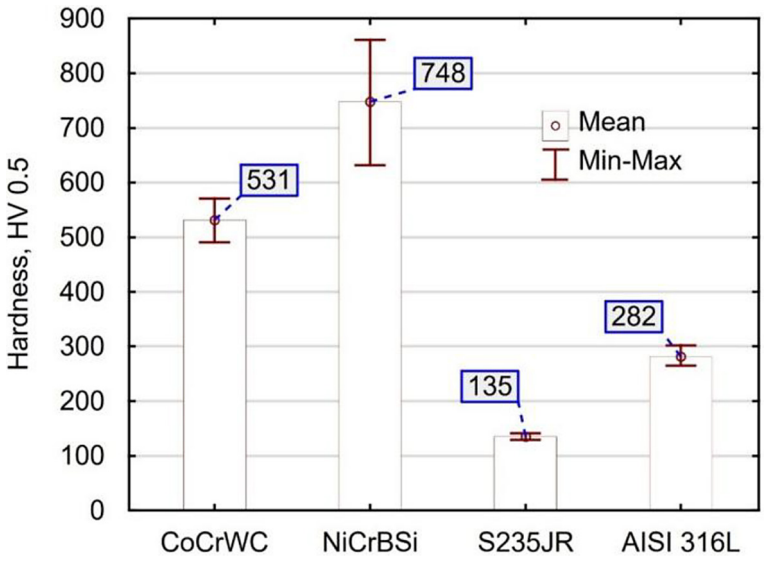

Figure 4. Surface hardness of the investigated hardfacings and steels

Analysis of cavitation erosion and tribological performance

The paper originally compares and reports the cavitation erosion resistance and the sliding wear resistance of popular cobalt (Stellite 6) and nickel-based (self-fluxing alloy) hardfacings and popular steels. Investigated metallic materials differ in microstructure and hardness. Cavitation erosion results, as presented in Figure 5 and Table 4, indicate that CoCrWC exhibits the highest erosion resistance, followed by NiCrBSi, AISI 316L, and S235JR steels. Figure 6 compares the overview of eroded surfaces. It is clearly visible that the CoCrWC hardfacing exhibits minimal surface erosion, whereas the other tested samples display the typical cavitation erosion cauliflower morphology. Therefore, the erosion rate of the CoCrWC coatings ($MDER_{max}$ = 0.23 μm·h^{-1}, Figure 5b) was lowest among the tested materials, and its incubation period of erosion lasted approximately 15 hours (Figure 5c), which was really long in comparison to stellites manufactured by other techniques, such as HIPed Stellite 6 [68], the high-velocity oxy-fuel (HVOF) technique deposited Stellite 6 [69] or high entropy alloys $AlCoCrFeNiMo_x$ [70] and $AlCoCr_xCuFe$ [71]. Macrophotos of eroded surfaces show the lowest surface damage of CoCrWC observed at final times of exposure, in comparison to other tested samples, see Figure 6. The superior cavitation erosion resistance of Stellite 6 is attributed to its phase transformation and strain energy [48]. Figure 7a shows that at initial stages of erosion the cavitation erosion is initiated at carbides region, because the matrix is strengthened by the strain-induced phase transformation in the matrix i.e. cavitation loads induce phase transformations (e.g., face-centered cubic (fcc) to hexagonal close-packed (hcp) in the cobalt-based matrix) and the cavitation loads are absorbed by the formation of twins in the cobalt based matrix [72,73]. At further exposure time, the debonding of carbides results in the removal of cavitation-affected cobalt-based matrix. Therefore, erosion progresses, and pits and cracks form, as shown in Figure 7b.

The maximum erosion rate of the NiCrBSi was more than 8 times higher than that of CoCrWC, and the $MDER_{max}$ of AISI 316L and S235JR steel was noted to be 37- and 191 times higher than those reported for CoCrWC, respectively (see Table 4). NiCrBSi deposited via oxy-acetylene powder method has a slightly higher depth of erosion at 6 hours of exposure than those reported for comparable hardfacings deposited via powder plasma transferred arc welding (PPTAW) [74] and almost three times higher mass loss than those reported for flame-sprayed and further oxy-flame remelted the NiCrBSi and NiCrBSi/WC composite coatings [75]. Unlike the cobalt-based coating, there was no phase transformation for the nickel-based coating during the cavitation erosion, which was also reported by Hu et al. [56]. Figure 6 visualised the cauliflower-like erosion of NiCrBSi, comparable to damaged surfaces of steels observed at earlier exposure times. Analysis of microstructure before (Figure 3b) and after (Figure 7c,d) erosion testing confirms that at the incipient stage of erosion (Figure 7c), the

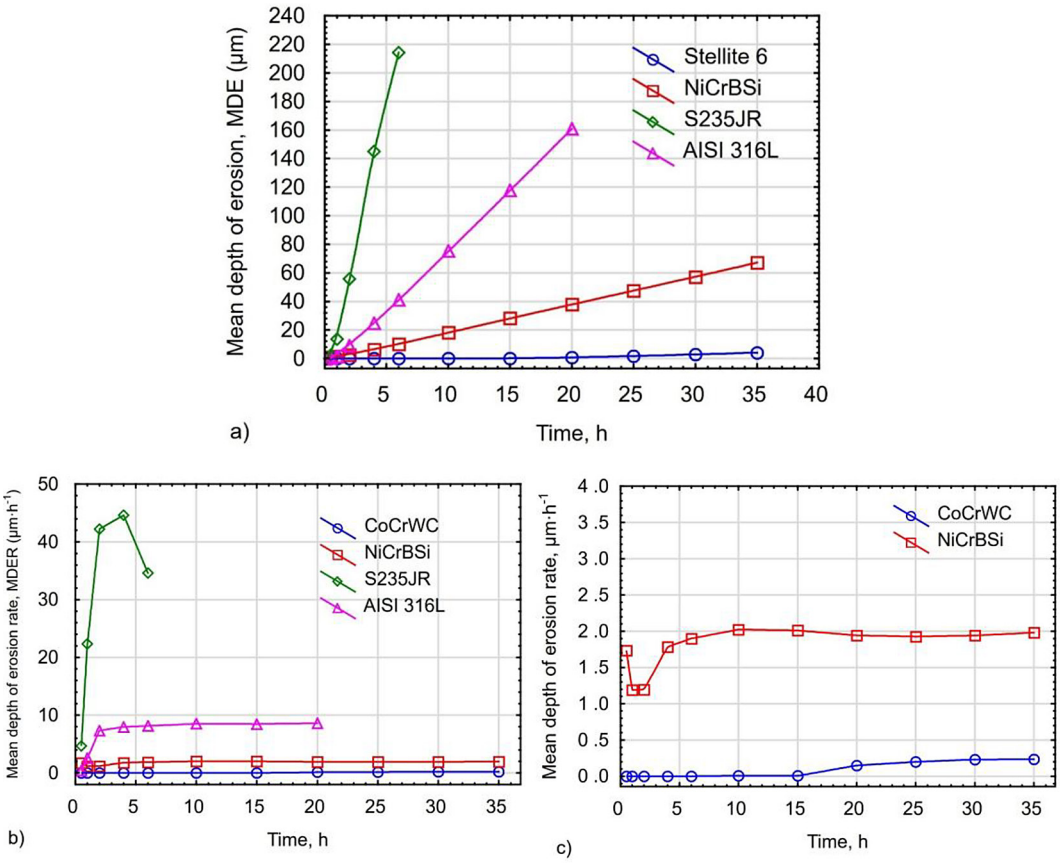

Figure 5. Cavitation erosion results: a) material loss (MDE), b) erosion rate (MDER), c) enlarged area of CoCrWC and NiCrBSi hardfacings erosion rates

cavitation erosion results in plastic deformation of the nickel-based matrix, which is strengthened by the presence of hard phases (carbides, borides, etc.). Generally, the exposed to cavitation loads, the multiphase microstructure of NiCrBSi coating undergoes selective erosion initiated at phase interfaces. The cavitation erosion of NiCrBSi progresses in two modes: first, erosion is initiated by the metallic matrix deformation and removal, and the second depends on the removal of hard phases located in the clusters. Clustered hard phases removal at the initial stages of erosion resulted in an increase in the erosion rate, noted at a few minutes of exposure to cavitation (Figure 5c), and cavitation pits were observed in Figure 7. Once the interface is deformed and eroded, the hard particles lose their anchor in the metallic matrix and are progressively removed (Figure 7c). Therefore, the surface shows the cracks, deep pits, craters and exposed protruding hard particles (Figure 7d) and both CoCrWC and NiCrBSi surfaces show fatigue-induced erosion. It seems that optimisation of the size, distribution and morphology of the hard particles embedded in the nickel-based matrix could facilitate the NiCrBSi cavitation erosion.

Table 4. Summary of the cavitation erosion results of the investigated materials

Sample	MDE_{6h} (µm)	$MDER_{max}$ (µm · h^{-1})
CoCrWC	0.00	0.23
NiCrBSi	10.03	2.02
S235JR	214.26	44.63
AISI 316L	41.17	8.63

In comparison to cobalt and nickel-based coatings, steels present lower cavitation erosion resistance (Fig. 5a,b). Exemplifying this, MDE material loss noted after 6 hours of exposure to cavitation was the highest for S235JR > AISI 316L > NiCrBSi > CoCrWC (Table 4). The mild steel shows the accelerated erosion; therefore, the tests have been stopped after 6 hours of exposure. The damaged surface, as shown in Figure 8, exhibits deep pits and even 80 µm large craters and cracks, resulting from material fatigue due to cavitation (Fig. 8b). Therefore, for carbon steel, erosion occurs first in ferrite and then in pearlite,

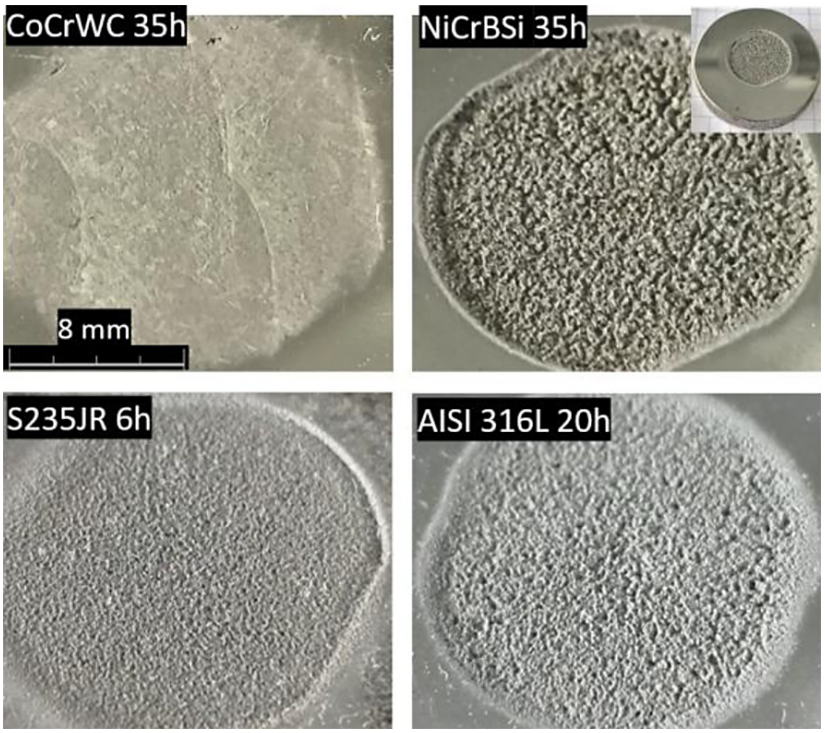

Figure 6. Macrophotos of the eroded surfaces (different total times of exposure to cavitation)

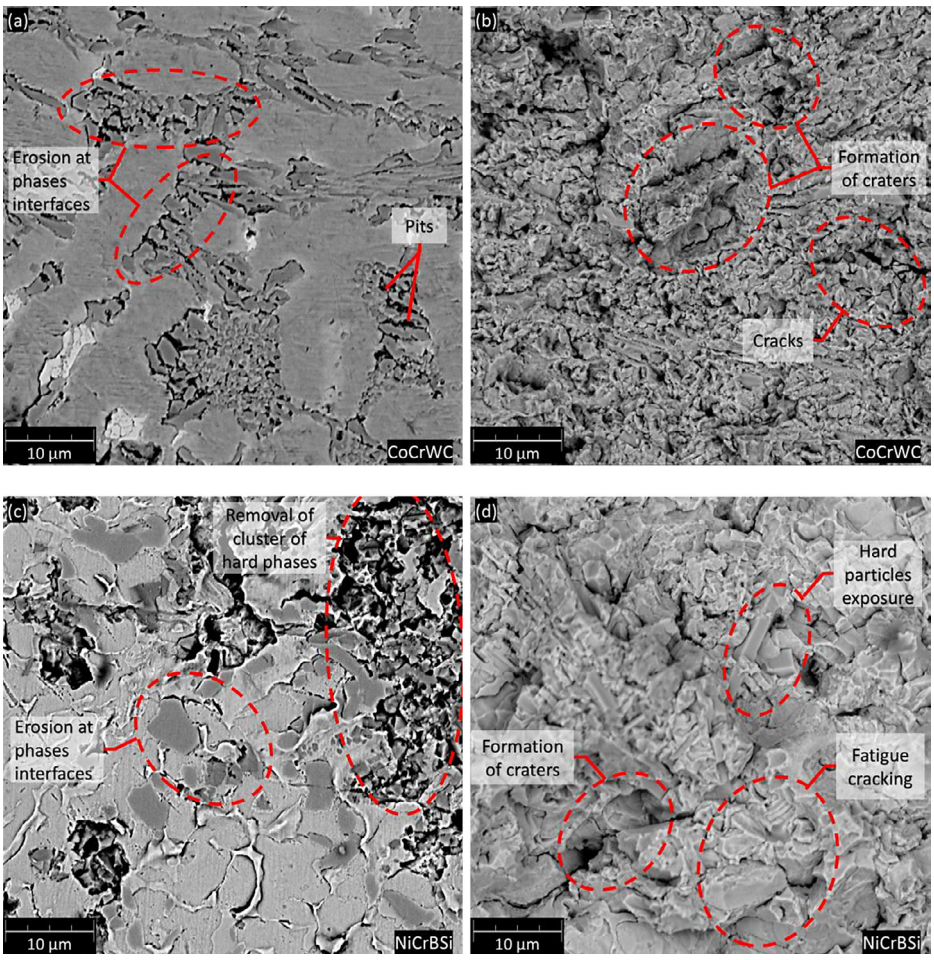

Figure 7. Eroded surfaces of CoCrWC (a, b) and NiCrBSi (c, d) hardfacings observed at initial stages of erosion (a and c) and after 35 hours of exposure to cavitation (b and d), mag. x1000 and x5000, SEM

which is in agreement with findings of Hattori et al. [52,76]. The corrosion and fatigue resistance of stainless steel is much higher than that reported for mild steel [77,78]; therefore, the AISI 316 steel withstands much longer exposure time than S235JR steel which is proved by the cavitation erosion results given in Figure 5a. Obtained material loss was higher than those reported in other experiments for AISI 316L bulk steel [65] or powder plasma transferred arc deposited AISI 316L hardfacings [74]. Generally, the austenitic stainless steel cavitation erosion resistance is attributed to its strain hardening ability of austenite and induction of martensitic transformation under cavitation loads [64]. On the other hand, the stability of the austenite phase of SUS316 is higher than that of SUS304, making it challenging to generate the stress-induced martensite phase [52]. The microscopic observation of eroded surfaces is shown in Figure 9, confirming the pits, craters, and cracks caused by the fatigue action of cavitation erosion. Overall, the fatigue action of cavitation is a dominant mode of erosion of metallic engineering materials [2,79,80].

The analysis of the results indicates that there is no direct correlation between the hardness and cavitation erosion resistance of the tested materials. Conversely, soft materials, such as tested steels, demonstrate lower erosion resistance compared to hard hardfacings. Finally, it can be confirmed that hardness cannot be the primary and sole factor influencing cavitation erosion

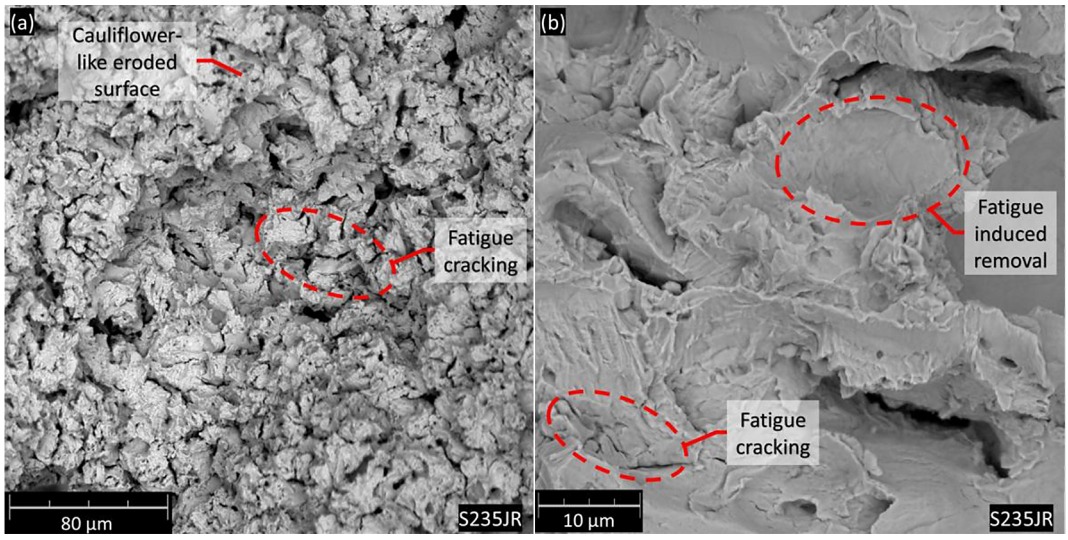

Figure 8. Eroded surfaces of S235JR mild steel after 6 hours of exposure, mag. x1000 and x5000, SEM

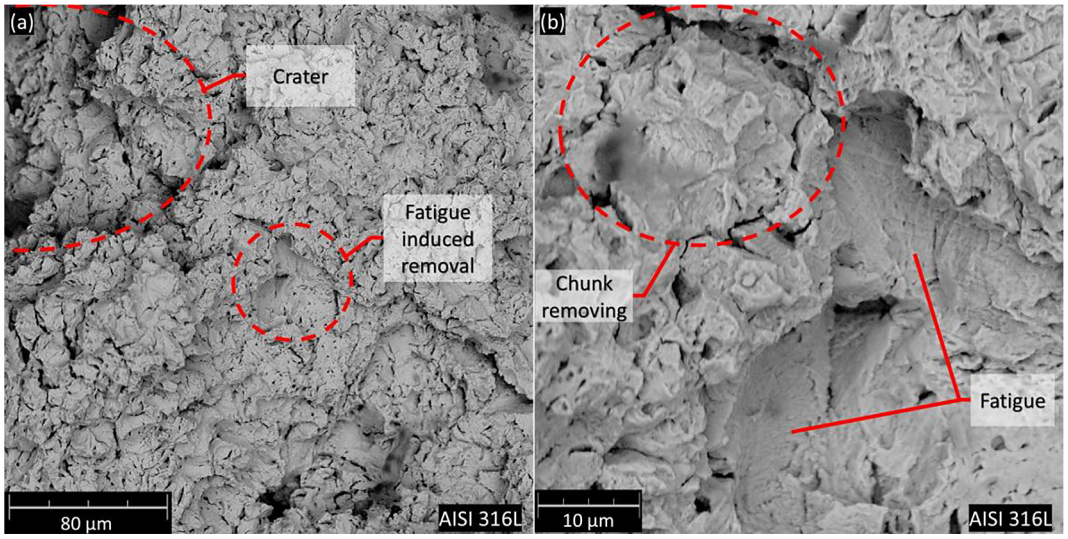

Figure 9. Eroded surfaces of AISI 316L stainless steel after 20 hours of exposure, mag. x1000 and x5000, SEM

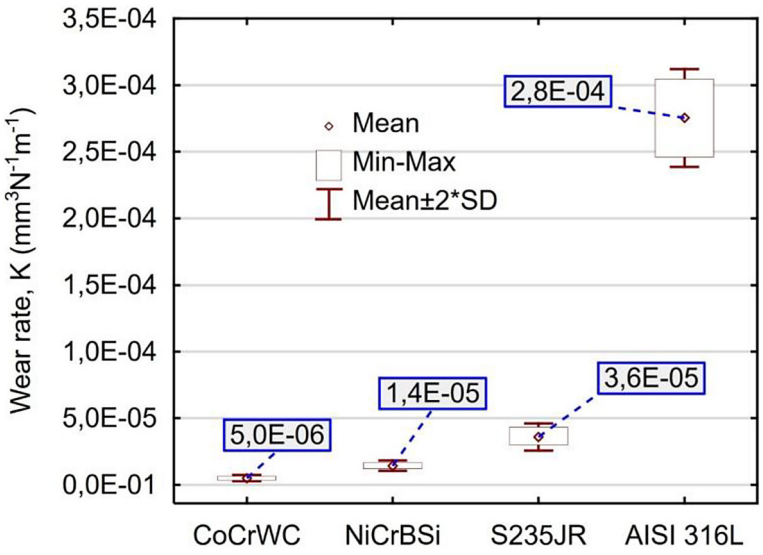

Figure 10. The wear rate *K* of CoCrWC and NiCrBSi hardfacings, S235JR mild steel and AISI 316L stainless steel

resistance, and metallic materials with different chemical compositions exhibit distinct cavitation erosion mechanisms. These mechanisms strongly depend on the material properties, as it was signalled in a previous paper [61] proposing the qualitative relationship for estimating the cavitation erosion damage (CE_d) of a selected group of metallic materials.

The idea of this paper is to comparatively present the cavitation erosion results and the sliding wear resistance of different metallic materials. The lowest material loss and highest wear resistance were noted in the following order: CoCrWC > NiCrBSi > S235JR > AISI 316L (Figure 10). While the S235JR steel shows the lowest friction coefficient, other samples had COF noted at a comparable level, Table 5. The highest wear resistance of hardfacings is attributed to relatively high hardness (Figure 4) and can be explained by the analysis of the wear mechanisms using SEM (Figure 11). The hardness of 100Cr6 (64HRC) is comparable to that of NiCrBSi and CoCrWC hardfacings, and more than twice that of the investigated steels. The hard carbide eutectics in the cobalt matrix of the CoCrWC coating, along with the presence of second phases in the nickel-based matrix of NiCrBSi, minimise material loss. This, in turn, allows the 100Cr6 counterball to slide over the top, reducing the abrasive action of nickel- and cobalt-based matrix. The observations of wear tracks indicate that the abrasive wear debris produced is oxidised, smashed through the wear track, and undergoes fatigue. The areas free from wear debris are also observed in the wear tracks of both hardfacings (Figure 11), in contrast to steels' wear tracks, which are rich in abrasive wear products (Figure 12 and 13), and end up in an adhesive wear mechanism. The hard counterball embedded in a ferrous matrix results in smashing the material and forming a tribofilm, which is comparable to findings given in [12]. The difference between the wear of S235JR and AISI 316L relies on the formation of a compact tribofilm made of wear products of S235JR (Figure 12), contrary to wear debris oxidising and further spallation in the case of AISI 316L stainless steel (Figure 13). Thus, higher wear resistance is noted in the case of the ferritic-pearlitic S235JR sample. The stainless steel AISI 316L has the highest material loss (Figure 10). Similar results were obtained in [81] for a 16 kg load, where SS304 shows the highest wear rate, whereas mild steel shows a comparatively very slow wear rate. This might be because it has a high amount of carbon [81]. On the contrary, in the work [82] the mild steel obtained the highest wear rate and COF in comparison to stainless steel. The coefficient of friction of 316L and 100Cr6 counterball (Table 5) was in

Table 5. Coefficient of friction (COF) of materials

Sample	Average COF	Standard deviation
CoCrWC	0.605	0.069
NiCrBSi	0.698	0.122
S235JR	0.467	0.041
AISI 316L	0.641	0.086

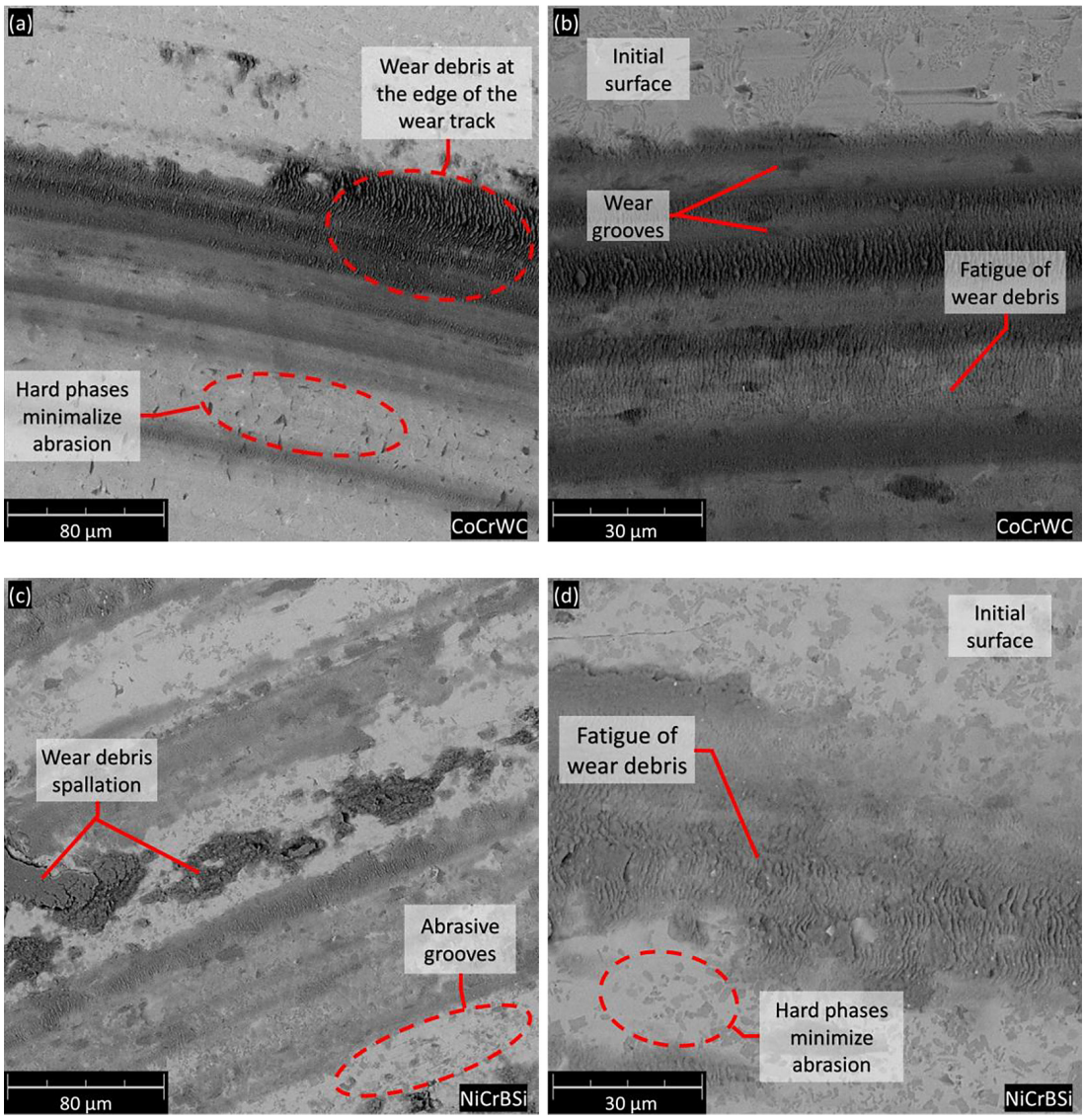

Figure 11. The wear mechanisms of hardfacings: a, b – CoCrWC, c d – NiCrBSi, mag. x1000 and x2500, SEM

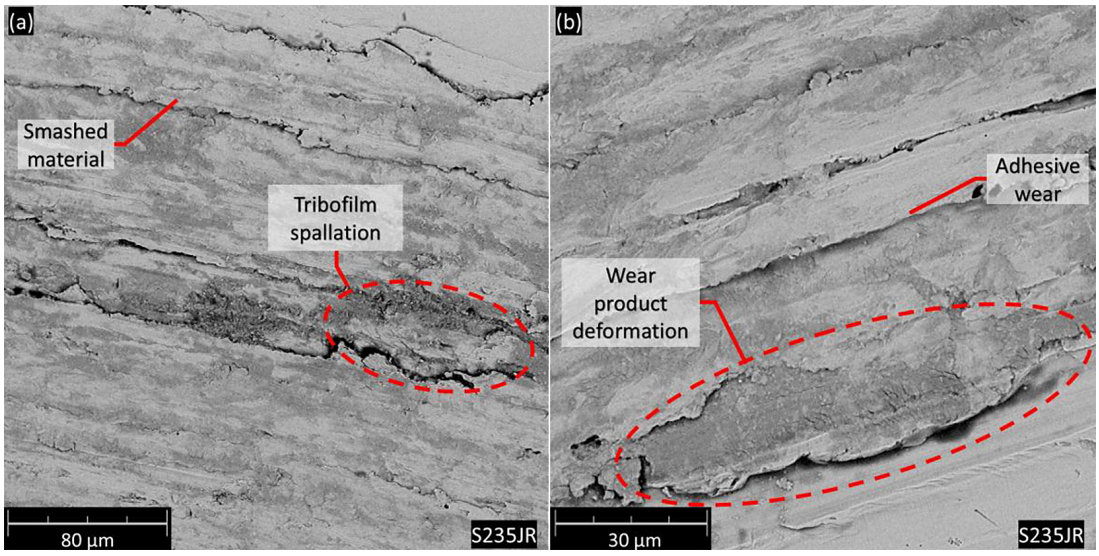

Figure 12. Analysis of the wear mechanisms of S235JR mild steel (a,b). mag. x1000 and x2500, SEM

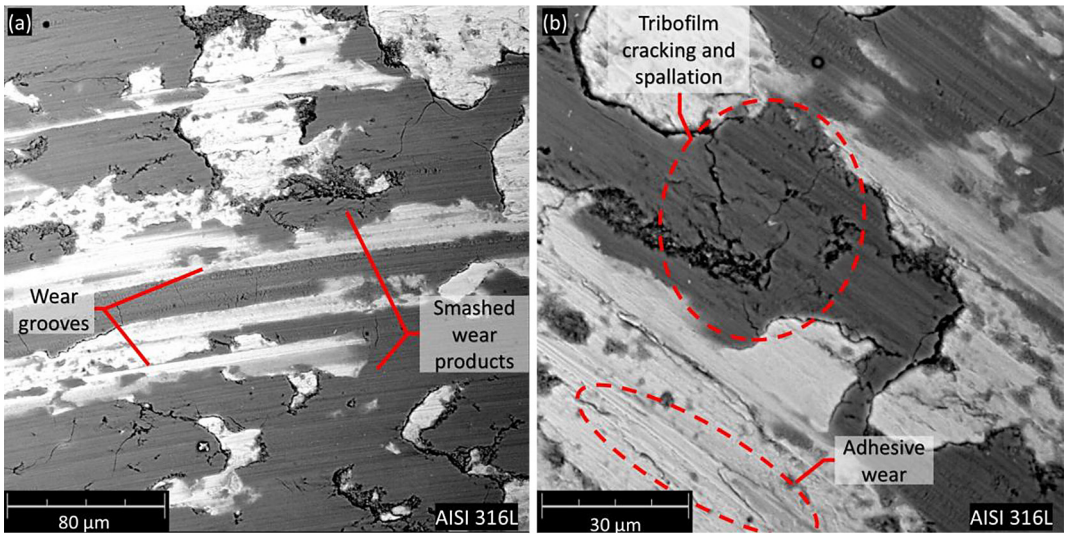

Figure 13. Analysis of the wear mechanisms of AISI 316L stainless steel (a, b), mag. x1000 and x2500, SEM

the range of those resented for sliding of stainless steels with other counterballs noted at the level of COF = 0.603 [62] and COF = 0.697 [83] for WC-Co (hardness 1900HV0.5) and differs from those reported for Al_2O_3 counterball (hardness 1675 HV0.5) COF = 0.452 [70]. Generally, sliding velocity as well a applied load increases wear rate [84,85]. So, depending on the tribological conditions and friction pair selection, the achieved COF and wear rates can be obtained for the same material.

The comparative analysis of the results indicates that there is no direct correlation between the hardness and resistance to cavitation erosion and sliding wear of the tested materials. On the other hand, both the microstructure effect and the ratio of material hardness to countersample hardness play the decisive role; therefore, materials dominated by a single-phase microstructure, which are relatively soft, show high sliding wear material loss.

CONCLUSIONS

The main objective of the study was to comparatively analyse the cavitation erosion resistance and dry sliding wear resistance of two popular steels – S235JR mild steel (approx. 0.17% C) and stainless steel (AISI 316L) – as well as two hardfacing alloys: NiCrBSi (a self-fluxing alloy) and CoCrWC (Stellite 6). The investigation yielded the following conclusions:

- CoCrWC hardfacing exhibits the highest resistance to cavitation erosion and sliding wear, surpassing by several times the performances reported for NiCrBSi and being substantially greater than those for steels.
- Cavitation erosion decreased in the following order CoCrWC > NiCrBSi > AISI 316L > S235JR. Consequently, the maximum depth of erosion rate ($MDER_{max}$) of NiCrBSi hardfacing (2.02 µm·h^{-1}), AISI 316L stainless steel (8.63 µm·h^{-1}), and S235JR mild steel (44.63 µm·h^{-1}) was approximately 8, 37, and 191 times higher, respectively, than that of CoCrWC ($MDER_{max}$ = 0.23 µm·h^{-1}).
- Sliding wear resistance follows this order, starting with the highest: CoCrWC > NiCrBSi > S235JR > AISI 316L, while the lowest COF = 0.467 was observed for S235JR, with other samples showing comparable COF values in the range 0.605–0.698.
- The general conclusion can be drawn that both the microstructure effect and the ratio of material hardness to counterball hardness play the decisive role; therefore, materials dominated by a single-phase microstructure, which are relatively soft, show high material losses in sliding wear and cavitation erosion tests.
- The cavitation erosion resistance depends on the material's ability to absorb cavitation loads through the metallic matrix and is also influenced by material fatigue. Erosion in all tested materials begins with the deformation of grains and phase interfaces and advances through the detachment of deformed material. In the

case of hardfacings, once the hard carbides, borides, etc., lose their restraint, they are removed. Ultimately, erosion progresses via the formation of pits, craters, and cracks caused by fatigue-induced material detachment.

- The sliding wear mechanisms depend on microstructure. In the case of sliding wear, embedded hard particles in the metallic matrix reduce material loss by minimising the counterball abrasive action. Steel has a relatively soft metallic matrix, and the dominance of a single-phase structure results in abrasive wear debris leading to an adhesive wear mechanism, which increases wear rates and decreases wear resistance. The stainless steel AISI 316L shows the highest sliding wear material loss, exceeding that of S235JR steel. This can be explained by the formation of wear products that oxidise and spall from the wear track of AISI 316L, compared to the well-adhered tribofilm of S235JR steel.
- The analysis of the results shows that there is no direct correlation between resistance to cavitation erosion and the sliding wear of the tested materials.

Acknowledgements

VIA CARPATIA Universities of Technology Network named after the President of the Republic of Poland Lech Kaczyński" under the special purpose grant from the Minister of Education and Science, contract no. MEiN/2022/DPI/2575, as part of the action "In the neighborhood – inter-university research internships and study visits".

REFERENCES

1. Singh J., Hashmi A.W., Review on fluid forces and their action on centrifugal pump impeller, Int. J. Interact. Des. Manuf. IJI31DeM 19 2025; 1611–1631. https://doi.org/10.1007/s12008-024-02109-1
2. Krella A.K., Degradation and protection of materials from cavitation erosion: a review, Materials 2023; 16 2058. https://doi.org/10.3390/ma16052058
3. Surkar H.S, Kumar A., Sirohi S., Pandey S.M., Świerczyńska A., Fydrych D., Pandey C., A dissimilar welded joint of grade 92 steel and AISI 304L steel obtained using IN82 buttering and IN617 filler: relationship of microstructure and mechanical properties, Arch. Civ. Mech. Eng. 2024; 24 109. https://doi.org/10.1007/s43452-024-00920-x
4. Gradzik A., Walczyk K., Gancarczyk K., Kościelniak B., Walczak M., Gancarczyk N., Nawrocki J., Albrecht R., Influence of high-temperature substrate preheating on laser cladding of Stellite 6 onto Inconel 718 alloy, Materials 2025; 18: 1814. https://doi.org/10.3390/ma18081814
5. Younes R., Tomków J., Skowrońska B., Bradai M.A., Characteristics of AISI 420 And AISI 301 stainless steels coatings obtained by thermal spraying, Adv. Mater. Sci. 2025; 25: 95–111. https://doi.org/10.2478/adms-2025-0006
6. Mitelea I., Bordeașu I., Mutașcu D., Crăciunescu C.M., Uțu I.D., Surface integrity of austenitic manganese alloys hard layers after cavitation erosion, Lubricants 2024; 12: 330. https://doi.org/10.3390/lubricants12100330
7. Ning Y., Qiu Z., Wu B., Pan Z., Li H., Hardfacing of metals: A review of consumables, properties and strengthening processes, J. Mater. Res. Technol. 2025; 36: 6330–6349. https://doi.org/10.1016/j.jmrt.2025.04.221
8. Trembach B., Silchenko Y., Balenko O., Hlachev D., Kulahin K., Heiko H., Bellorin-Herrera O., Khabosha S., Zakovorotnyi O., Trembach I., Study of the hardfacing process using self-shielding flux-cored wire with an exothermic addition with a combined oxidizer of the Al-(CuO/Fe_2O_3) system, Int. J. Adv. Manuf. Technol. 2024; 134: 309–335. https://doi.org/10.1007/s00170-024-14115-4
9. Mičian M., Gucwa M., Parzych S., Koňár R., Winczek J., The evaluation of the wear mechanism of high-carbon hardfacing layers, Arch. Metall. Mater. 2019; 64(3): 1111–1115. https://journals.pan.pl/dlibra/publication/129502/edition/113030 (accessed July 9, 2025).
10. Górnik M., Lachowicz M., Łatka L., Corrosion resistance of PPTA Ni-based hardfacing layers, Mater. Sci.-Pol. 2024; 42: 66–78. https://doi.org/10.2478/msp-2024-0040
11. Xu L., Kennon N.F., A study of the abrasive wear of carbon steels, Wear 1991; 148: 101–112. https://doi.org/10.1016/0043-1648(91)90209-D
12. Nedeloni L., Korka Z., Pascal D., Kazamer N., Nedeloni M., Comparative study on dry sliding wear resistance of carbon steel, alloyed steel and cast iron, in: 2018: 012026. https://doi.org/10.1088/1757-899X/416/1/012026
13. Pintaude G., Bernardes F.G., Santos M.M., Sinatora A., Albertin E., Mild and severe wear of steels and cast irons in sliding abrasion, Wear 2009; 267: 19–25. https://doi.org/10.1016/j.wear.2008.12.099
14. Szala M., Szafran M., Matijošius J., Drozd K., Abrasive wear mechanisms of S235JR, S355J2, C45, AISI 304, and Hardox 500 steels tested using garnet, corundum and carborundum abrasives, Adv. Sci. Technol. Res. J. 2023; 17: 147–160. https://doi.

org/10.12913/22998624/161277

15. Szala M., Łatka L., Nowakowska M., Kamiński M., Cavitation erosion and wet environment tribological behaviour of Al_2O_3–13% TiO_2 coatings deposited via different atmospheric plasma spraying parameters, Acta Phys. Pol. A 2022; 142733–740.
16. Özkan D., Yılmaz M.A., Bakdemir S.A., Sulukan E., Wear and friction behavior of TiB_2 thin film–coated AISI 52100 steels under the lubricated condition, Tribol. Trans. 2020; 631008–1019. https://doi.org/10.1080/10402004.2020.1784497
17. Özkan D., Yilmaz M.A., Karakurt D., Szala M., Walczak M., Bakdemir S.A., Türküz C., Sulukan E., Effect of AISI H13 steel substrate nitriding on AlCrN, ZrN, TiSiN, and TiCrN multilayer PVD coatings wear and friction behaviors at a different temperature level, Materials 2023; 16: 1594. https://doi.org/10.3390/ma16041594
18. Appiah A.N.S., Wyględacz B., Matus K., Reimann Ł., Bialas O., Batalha G.F., Czupryński A., Adamiak M., Microstructure and performance of NiCrBSi coatings prepared by modulated arc currents using powder plasma transferred arc welding technology, Appl. Surf. Sci. 2024; 648: 159065. https://doi.org/10.1016/j.apsusc.2023.159065
19. Mráz J., Bakalova T., The impact of cryogenic temperatures on the hardness and tribological properties of cobalt alloys, Manuf. Technol. 2024; 24: 626–635. https://doi.org/10.21062/mft.2024.057
20. Cui G., Cui H., Zhang W., Yan X., Li J., Kou Z., Wear performance of ZrO_2 reinforced Stellite 6 matrix coatings prepared by laser cladding at elevated temperature, Wear 2024; 556–557: 205539. https://doi.org/10.1016/j.wear.2024.205539
21. Budzyński P., Kamiński M., Turek M., Wiertel M., Impact of nitrogen and manganese ion implantation on the tribological properties of Stellite 6 alloy, Wear 2020; 456–457: 203360. https://doi.org/10.1016/j.wear.2020.203360
22. Kamiński M., Budzyński P., Szala M., Turek M., Tribological properties of the Stellite 6 cobalt alloy implanted with manganese ions, IOP Conf. Ser. Mater. Sci. Eng. 2018; 421: 032012. https://doi.org/10.1088/1757-899X/421/3/032012
23. Morozow D., Barlak M., Werner Z., Pisarek M., Konarski P., Zagórski J., Rucki M., Chałko L., Łagodziński M., Narojczyk J., Krzysiak Z., Caban J., Wear resistance improvement of cemented tungsten carbide deep-hole drills after ion implantation, Materials 2021; 14: 239. https://doi.org/10.3390/ma14020239
24. Güney B., Erden M.A., Effect of heat treatments on microstructural and tribological properties of 3d printed 18Ni-300 maraging tool steel made by selective laser sintering process, Sci. Sinter. 2025; 26–26.
25. Świetlicki A., Walczak M., Szala M., Effect of shot peening on corrosion resistance of additive manufactured 17-4PH steel, Mater. Sci.-Pol. 2022; 40: 135–151. https://doi.org/10.2478/msp-2022-0038
26. Kopec M., Gunputh U., Williams G., Macek W., Kowalewski Z.L., Wood P., Fatigue damage evolution in SS316L produced by powder bed fusion in different orientations with reused powder feedstock, Exp. Mech. 2025; 65: 427–442. https://doi.org/10.1007/s11340-024-01118-1
27. Capasso I., Andreacola F.R., Brando G., Additive manufacturing of metal materials for construction engineering: An overview on technologies and applications, Metals 2024; 14: 1033. https://doi.org/10.3390/met14091033
28. Müller C., Müller J., Kloft H., Hensel J., Design of structural steel components according to manufacturing possibilities of the robot-guided ded-arc process, Buildings 2022; 12: 2154. https://doi.org/10.3390/buildings12122154
29. Selvam S.K., Sanjeeviprakash K., Kannan A.R., Sankaranarayanasamy K., Shanmugam N.S., Characterization of microstructure, mechanical properties and machinability of stellite-6 hard-faced cutting tool for machining high-strength aluminum alloys, Proc. Inst. Mech. Eng. Part E J. Process Mech. Eng. 2025; 09544089251324566. https://doi.org/10.1177/09544089251324566
30. Zatloukal T., Řehoř J., Fulemova J., Povolny M., Optimization of the Machining Process of NiCrBSi Thermal Spraying, in: 2020; 0632–0637. https://doi.org/10.2507/31st.daaam.proceedings.087
31. Řehoř J., Gombár M., Harničárová M., Kušnerová M., Houdková-Šimůnková Š., Valíček J., Fulemová J., Vagaská A., Investigation of machining of Stellite 6 alloy deposited on steel substrate, Int. J. Adv. Manuf. Technol. 2022; 121: 889–901. https://doi.org/10.1007/s00170-022-09380-0
32. Lin Z., Ya W., Subramanian V.V., Goulas C., di Castri B., Hermans M.J.M., Pathiraj B., Deposition of Stellite 6 alloy on steel substrates using wire and arc additive manufacturing, Int. J. Adv. Manuf. Technol. 2020; 111: 411–426. https://doi.org/10.1007/s00170-020-06116-w
33. Bakhshayesh M.M., F. Khodabakhshi, M.H. Farshidianfar, Š. Nagy, M. Mohammadi, G. Wilde, Additive manufacturing of Stellite 6 alloy by laser-directed energy deposition: Engineering the crystallographic texture, Mater. Charact. 2024; 207: 113511. https://doi.org/10.1016/j.matchar.2023.113511
34. Łatka L., Biskup P., Development in PTA surface modifications – A Review, Adv. Mater. Sci. 2020; 20: 39–53. https://doi.org/10.2478/adms-2020-0009
35. Dilawary S.A.A., Motallebzadeh A., Atar E., Cimenoglu H., Influence of Mo on the high temperature wear performance of NiCrBSi hardfacings, Tribol. Int. 2018; 127: 288–295. https://doi.

org/10.1016/j.triboint.2018.06.022

36. Singh J., Singh S., Vasudev H., Katiyar J.K., Artificial neural network model for wear characteristic analysis of WC-10Co4Cr and Stellite 6 thermal spray coatings, Tribol. Int. 2024; 109924. https://doi.org/10.1016/j.triboint.2024.109924
37. Hajian M., Abdollah-zadeh A., Rezaei-Nejad S.S., Assadi H., Hadavi S.M.M., Chung K., Shokouhimehr M., Improvement in cavitation erosion resistance of AISI 316L stainless steel by friction stir processing, Appl. Surf. Sci. 2014; 308: 184–192. https://doi.org/10.1016/j.apsusc.2014.04.132
38. Santos L.L., Cardoso R.P., Brunatto S.F., Behavior of the reversed austenite in CA-6NM martensitic stainless steel under cavitation, Wear 2020; 454–455: 203322. https://doi.org/10.1016/j.wear.2020.203322
39. Świetlicki A., Walczak M., Szala M., Chocyk D., Nowak W.J., Effect of the shot peening finishing on cavitation erosion and corrosion resistance of DMLS manufactured 17-4PH steel, Eng. Fail. Anal. 2025; 110127. https://doi.org/10.1016/j.engfailanal.2025.110127
40. Qin Z., Li X., Xia D., Zhang Y., Feng C., Wu Z., Hu W., Effect of compressive stress on cavitation erosion-corrosion behavior of nickel-aluminum bronze alloy, Ultrason. Sonochem. 2022; 89: 106143. https://doi.org/10.1016/j.ultsonch.2022.106143
41. Ding X., Huang Y., Yuan C., Ding Z., Deposition and cavitation erosion behavior of multimodal WC-10Co4Cr coatings sprayed by HVOF, Surf. Coat. Technol. 2020; 392: 125757. https://doi.org/10.1016/j.surfcoat.2020.125757
42. Tian W., Guo Z., Wang S., Yu H., Wang S., Jin H., Tian L., Hydrogen and DA bond-based self-healing epoxy-modified polyurea composite coating with anti-cavitation, anticorrosion, antifouling, and strong adhesion properties, J. Mater. Sci. Technol. 2024; 187: 1–14. https://doi.org/10.1016/j.jmst.2023.11.031
43. Liu G., Zhang Y., Lian Z., Xu J., Wang J., Zhang M., Xue W., Liu H., Zhou J., Cavitation erosion performance and phase transformation strengthening behavior of laser clad iron-based shape memory alloy coatings, Mater. Today Commun. 2024; 41: 110184. https://doi.org/10.1016/j.mtcomm.2024.110184
44. Yöyler S., Surženkov A., Tarraste M., Kolnes M., Juhani K., Erosive wear of stainless steel-based hardfacings with ex-situ and in-situ synthesized TiC, Coatings 2025; 15: 658. https://doi.org/10.3390/coatings15060658
45. Szymański Ł., Olejnik E., Sobczak J.J., Szala M., Kurtyka P., Tokarski T., Janas A., Dry sliding, slurry abrasion and cavitation erosion of composite layers reinforced by TiC fabricated in situ in cast steel and gray cast iron, J. Mater. Process. Technol. 2022; 308: 117688. https://doi.org/10.1016/j.jmatprotec.2022.117688
46. Volkov-Husović T., Martinović S., Alil A., Vlahović M., Dimitrijević B., Ivanić I., Pavkov V., Comparative investigation of ultrasonic cavitation erosion for two engineering materials, J. Min. Metall. Sect. B Metall. 2024; 60: 295–304.
47. Tang X., Zhang S., Cui X., Zhang C., Liu Y., Zhang J., Tribological and cavitation erosion behaviors of nickel-based and iron-based coatings deposited on AISI 304 stainless steel by cold metal transfer, J. Mater. Res. Technol. 2020; 9: 6665–6681. https://doi.org/10.1016/j.jmrt.2020.04.064
48. Lee M., Kim Y., Oh Y., Kim Y., Lee S., Hong H., Kim S., Study on the cavitation erosion behavior of hardfacing alloys for nuclear power industry, Wear 2003; 255: 157–161. https://doi.org/10.1016/S0043-1648(03)00144-3
49. Levărdă E., Cîrlan D.-C., Chicet D.L., Petcu M., Toma S.L., Investigations on cavitation erosion and wear resistance of high-alloy WC coatings manufactured by electric arc spraying, Materials 2025; 18: 2259. https://doi.org/10.3390/ma18102259
50. Heathcock C.J., Protheroe B.E., Ball A., Cavitation erosion of stainless steels, Wear 1982; 81: 311–327. https://doi.org/10.1016/0043-1648(82)90278-2
51. Hattori S., Ishikura R., Zhang Q. Construction of database on cavitation erosion and analyses of carbon steel data, Wear 2004; 257: 1022–1029. https://doi.org/10.1016/j.wear.2004.07.002
52. Hattori S., Ishikura R., Revision of cavitation erosion database and analysis of stainless steel data, Wear 2010; 268: 109–116. https://doi.org/10.1016/j.wear.2009.07.005
53. Archard J.F., Contact and Rubbing of Flat Surfaces, J. Appl. Phys. 1953; 24: 981–988. https://doi.org/10.1063/1.1721448
54. Górka J., Poloczek T., Janicki D., Lont A., Topór S., Żuk M., Rzeźnikiewicz A., Microstructure and erosion wear of in situ TiC-reinforced Co-Cr-W-C (Stellite 6) laser-cladded coatings, Materials 2024; 17: 3101. https://doi.org/10.3390/ma17133101
55. Shahroozi A., Afsari A., Khakan B., Khalifeh A.R., Microstructure and mechanical properties investigation of stellite 6 and Stellite 6/TiC coating on ASTM A105 steel produced by TIG welding process, Surf. Coat. Technol. 2018; 350: 648–658. https://doi.org/10.1016/j.surfcoat.2018.07.044
56. M. E, Hu H.X., Guo X.M., Zheng Y.G., Comparison of the cavitation erosion and slurry erosion behavior of cobalt-based and nickel-based coatings, Wear 2019; 428–429: 246–257. https://doi.org/10.1016/j.wear.2019.03.022
57. Suthar F.V., Shah H.N., Mandal D., Chaudhury S.K., Effect of deposition current on microstructure, hardness and residual stress distribution of

NiCrBSiC hardfacing alloy, J. Mater. Eng. Perform. 2025; 34: 10080–10092. https://doi.org/10.1007/s11665-025-10674-z

58. Sun Q., Bi W., Yao S., Zhu W., Ma W., Hu B., Bao C., Zhang Y., Niu F., Effect of gradient transition layer on the cracking behavior of Ni60B (NiCrBSi) coatings by laser cladding, Materials 2025; 18: 419. https://doi.org/10.3390/ma18020419
59. Górka J., Lont A., Poloczek T., The microstructure and properties of laser-cladded Ni-based self-fluxing alloy coatings reinforced by TiC particles, Coatings 2025; 15: 527. https://doi.org/10.3390/coatings15050527
60. Appiah A.N.S., Bialas O., Żuk M., Czupryński A., Sasu D.K., Adamiak M., Hardfacing of mild steel with wear-resistant Ni-based powders containing tungsten carbide particles using powder plasma transferred arc welding technology, Mater. Sci.-Pol. 2022; 40: 42–63. https://doi.org/10.2478/msp-2022-0033
61. Szala M., Walczak M., Hejwowski T., Factors influencing cavitation erosion of NiCrSiB hardfacings deposited by oxy-acetylene powder welding on grey cast iron, Adv. Sci. Technol. Res. J. 2021; 15: 376–386. https://doi.org/10.12913/22998624/143304
62. Walczak M., Surface characteristics and wear resistance of 316L stainless steel after different shot peening parameters, Adv. Sci. Technol. Res. J. 2023; 17: 124–132. https://doi.org/10.12913/22998624/165800
63. Nowak W.J., Kubaszek T., Gradzik A., Grądzka-Dahlke M., Perkowski D., Tokarewicz M., Walczak M., Szala M., Effect of Ti doping of Al0.7CoCrFeNi-based high entropy alloys on their erosion resistance by solid particles, Materials 2025; 18: 3328. https://doi.org/10.3390/ma18143328
64. Abedini M., Lopez de Arcaute y Lozano C., Kostka A., Hanke S., Influence of surface finishing by grinding on the cavitation erosion resistance of 316L and NiAl-bronze, Wear 2024; 554–555: 205432. https://doi.org/10.1016/j.wear.2024.205432
65. Lu P., Xu Z., Tian Y., Yang R., Hu K., Li H., Yin Y., Chen X., Effect of initial surface scratches on the cavitation erosion behavior of 316L stainless steel substrates and 316L stainless steel coatings, Materials 2023; 16: 1392. https://doi.org/10.3390/ma16041392
66. Lin C., Zhao Q., Zhao X., Yang Y., Cavitation erosion of metallic materials, Int. J. Georesources Environ. - IJGE Former. Intl J Geohazards Environ. 2018; 4: 1–8. https://doi.org/10.15273/ijge.2018.01.001
67. Stachowiak G., Batchelor A.W., Engineering Tribology, 4 edition, Butterworth-Heinemann, 2016.
68. Szala M., Chocyk D., Turek M., Effect of manganese ion implantation on cavitation erosion resistance of HIPed Stellite 6, Acta Phys. Pol. A 2022; 142: 741–746. https://doi.org/10.12693/APhysPolA.142.741
69. Lavigne S., Pougoum F., Savoie S., Martinu L., Klemberg-Sapieha J.E., Schulz R., Cavitation erosion behavior of HVOF CaviTec coatings, Wear 2017; 386–387: 90–98. https://doi.org/10.1016/j.wear.2017.06.003
70. Walczak M., Nowak W.J., Szala M., Grądzka-Dahlke M., Maciaszek N., Vališ D., Pasierbiewicz K., Effect of molybdenum addition on microstructure and behavior of AlCoCrFeNi high-entropy alloys in wet environments, Arch. Civ. Mech. Eng. 2025; 25: 205. https://doi.org/10.1007/s43452-025-01260-0
71. Yin D., Liang G., Fan S., Li S., Ultrasonic cavitation erosion behavior of AlCoCrxCuFe high entropy alloy coatings synthesized by laser cladding, Materials 2020; 13: 4067. https://doi.org/10.3390/ma13184067
72. Szala M., Phenomenological model of cavitation erosion of nitrogen ion implanted HIPed Stellite 6, Adv. Mater. Sci. 2023; 23: 98–109. https://doi.org/10.2478/adms-2023-0007
73. Kashani H., Amadeh A., Ohadizadeh A., Effect of temperature on the strain induced γ→ε phase transformation in Stellite 21 during wear test, Mater. Sci. Eng. A 2006; 435–436: 474–477. https://doi.org/10.1016/j.msea.2006.07.022
74. Henzler W., Szala M., Pałka T., Wyględacz B., Czupryński A., Łatka L., Comparison of cavitation erosion of NiCrBSi and AISI 316L coatings deposited by powder plasma transferred arc welding, Acta Polytech. 2025; 65: 282–287. https://doi.org/10.14311/AP.2025.65.0282
75. Ciubotariu C.-R., Frunzaverde D., Marginean G., Investigations of cavitation erosion and corrosion behavior of flame-sprayed NiCrBSi/WC-12Co composite coatings, Materials 2022; 15: 2943. https://doi.org/10.3390/ma15082943
76. Hattori S., Kitagawa T., Analysis of cavitation erosion resistance of cast iron and nonferrous metals based on database and comparison with carbon steel data, Wear 2010; 269: 443–448. https://doi.org/10.1016/j.wear.2010.04.031
77. Krella A.K., Zakrzewska D.E., Marchewicz A., The resistance of S235JR steel to cavitation erosion, Wear 2020; 452–453: 203295. https://doi.org/10.1016/j.wear.2020.203295
78. Rajput A., Ramkumar J., Mondal K., Cavitation resistance of a Cr-Mn stainless steel, a mild steel, and a high-carbon steel based on rust protectivity and corrosion behavior, J. Mater. Eng. Perform. 2022; 31: 439–447. https://doi.org/10.1007/s11665-021-06162-9
79. Okuniewski W., Walczak M., Szala M., Chocyk D., Effect of surface modification by shot peening

on cavitation erosion resistance of titanium alloy Ti-6Al-4V produced by DMLS method, Eng. Fail. Anal. 2025; 176: 109653. https://doi.org/10.1016/j.engfailanal.2025.109653

80. Sreedhar B.K., Albert S.K., Pandit A.B., Cavitation damage: Theory and measurements – A review, Wear 2017; 372–373: 177–196. https://doi.org/10.1016/j.wear.2016.12.009
81. Godse R.S., Gawande S.H., Keste A.A., Tribological behavior of high fraction carbon steel alloys, J. Bio- Tribo-Corros. 2016; 2: 3. https://doi.org/10.1007/s40735-016-0034-3
82. Chowdhury M., Nuruzzaman D., Experimental investigation on friction and wear properties of different steel materials, Tribol. Ind. 2013; 35: 42–50.
83. Szala M., Łatka L., Walczak M., Winnicki M., Comparative study on the cavitation erosion and sliding wear of cold-sprayed Al/Al_2O_3 and Cu/Al_2O_3 coatings, and stainless steel, aluminium alloy, copper and brass, Metals 2020; 10: 856. https://doi.org/10.3390/met10070856
84. Lim S.C., Ashby M.F., Overview no. 55 Wear-Mechanism maps, Acta Metall. 1987; 35: 1–24. https://doi.org/10.1016/0001-6160(87)90209-4
85. Nuruzzaman D.M., Chowdhury M.A., Friction coefficient and wear rate of different materials sliding against stainless steel, Int. J. Surf. Eng. Interdiscip. Mater. Sci. IJSEIMS 2013; 1: 33–45. https://doi.org/10.4018/ijseims.2013010103